PHOTOELECTROCHEMICAL PROPERTIES OF TITANIUM DIOXIDE NANOSTRUCTURES GROWN BY HYDROTHERMAL TECHNIQUE

FENG TAIXIANG

UNIVERSITI SAINS MALAYSIA

2025

PHOTOELECTROCHEMICAL PROPERTIES OF TITANIUM DIOXIDE NANOSTRUCTURES GROWN BY HYDROTHERMAL TECHNIQUE

by

FENG TAIXIANG

Thesis submitted in fulfilment of the requirements
for the degree of
Doctor of Philosophy

February 2025

ACKNOWLEDGEMENT

I am very grateful to my supervisor, Assoc. Prof. Dr. F. K. Yam, for giving me the opportunity to accomplish the PhD research in the exciting field of nanostructured oxide semiconductor materials for photoelectrochemical applications. Uncountable thanks for his patience, encouragement and wise supervision throughout my PhD research career. Besides, I greatly appreciate my supervisor providing his personal laboratory 335 for us to do the experiment, where most of my data collected from. And great thanks to the seniors working in Laboratory 335 for their various academic feedback. Furthermore, I would like to express my gratitude to the staff in Nano-Optoelectronics Research and Technology (NOR) Laboratory, School of Physics, Universiti Sains Malaysia (USM) for the characterization of my samples. Then, I would like to acknowledge and thank the Ministry of Higher Education Malaysia for Fundamental Research Grant Scheme with Reference Code: (FRGS/1/2020/STG05/USM/02/4), and Universiti Sains Malaysia (USM) for financial and technical support for this work. Also, I am very thankful to my parents for their financial and mental support in my PhD study. Without them I cannot get the achievement in the field. Thanks a lot, to my parents for being there for me anytime I needed them. Finally, I have been fortunate to take a Chinese girl, Wang Ting, as my neighbour who gives me the courage to accomplish the challenging PhD candidate during the epidemic of Covid-19. Thanks for the mental support from the young girl. I hope you can realize the difference you make in my life.

TABLE OF CONTENTS

ACKNOWLEDGEMENT ..... **ii**

TABLE OF CONTENTS ..... **iii**

LIST OF TABLES ..... **vii**

LIST OF FIGURES ..... **viii**

LIST OF SYMBOLS ..... **xiv**

LIST OF ABBREVIATIONS ..... **xvi**

ABSTRAK ..... **xviii**

ABSTRACT ..... **xx**

CHAPTER 1 INTRODUCTION **1**

1.1 Introduction 1

1.2 Motivation and Problem Statement 6

1.3 Research Objectives 10

1.4 Research Contribution 10

1.5 Thesis Outline 11

CHAPTER 2 BACKGROUND AND LITERATURE REVIEW **14**

2.1 Introduction 14

2.2 Titanium dioxide 15

2.2.1 History of Titanium dioxide 16

2.2.2 Titanium dioxide polymorphs 18

2.2.3 Structural properties of titanium dioxide 19

2.2.4 Optical properties of titanium dioxide 21

2.2.5 Features of titanium dioxide of different dimensions 26

2.2.6 Electronic properties of titanium dioxide 28

2.3 Fabrication methods of TiO_2 nanostructures 33

2.3.1 Anodization technique 33

2.3.2 Template assisted method 36
2.3.3 Chemical Vapor Deposition method 37
2.3.4 Sol-gel method 38
2.3.5 Hydrothermal method 38
2.3.5(a) Hydrothermal treatment 40
2.3.5(b) Acid washing 41
2.3.5(c) Thermal annealing 41
2.3.5(d) Discussion on Formation mechanism 42
2.4 Modification strategies 45
2.4.1 Metal doping 46
2.4.2 Nonmetal doping 47
2.4.3 Heterojunction formation 48
2.4.4 Annealing in a Reduction Environment 50
2.4.5 Synergistic Modification Strategies 51
2.5 Water splitting for Hydrogen generation 51
2.5.1 Basic mechanism for PEC Water Splitting 53
2.5.2 Photoelectrode material requirements 56
2.5.2(a) Bandgap of the material 56
2.5.2(b) Band edge positions 57
2.5.2(c) Chemical stability 58
2.5.3 Interfacial charge transfer 59
2.5.4 Quantification of hydrogen generation 63
2.6 Overview of Photocatalytic (PC) and photoelectrochemical (PEC) Water Splitting 64
2.6.1 Overview of related works on photocatalytic Water Splitting using TiO_2 based catalysts 64
2.6.2 Overview of related works on photoelectrochemical Water Splitting using TiO_2 based catalysts 71

CHAPTER 3 METHODOLOGY AND INSTRUMENTATION 81

3.1 Introduction 81

3.2 Experimental setup 83

3.2.1 Oven 83

3.2.2 Thermal annealing furnace 84

3.3 Hydrothermal synthesis of TiO_2 nanostructures 84

3.3.1 Starting materials 86

3.3.2 Ti foils cleaning 86

3.3.3 Hydrothermal treatment for Ti foils 86

3.3.4 Hydrochloric acid washing and annealing 86

3.4 Materials Characterization Techniques 87

3.4.1 Field-Emission Scanning Electron Microscope (FESEM) 87

3.4.2 Energy dispersive X-ray spectroscopy (EDX) 89

3.4.3 Structural analysis by X-ray diffraction (XRD) 90

3.4.4 UV-Vis-NIR spectrophotometer 92

3.4.5 Photoelectrochemical Characterization using Gamry Potentiostat 93

CHAPTER 4 RESULTS AND DISCUSSION: PHYSICAL PROPERTIES OF THE TiO_2 NANOSTRUCTURES 96

4.1 Introduction 96

4.2 Effect of hydrothermal treatment duration 96

4.2.1 Morphological properties 97

4.2.2 Structural properties 101

4.2.3 Optical properties 102

4.3 Effect of hydrothermal treatment temperature 104

4.3.1 Morphological properties 105

4.3.2 Structural properties 108

4.3.3 Optical properties 111

4.4 Summary 112

CHAPTER 5 RESULTS AND DISCUSSIONS PHOTOELECTROCHEMICAL PROPERTIES FOR THE TiO_2 NANOSTRUCTURES 115

5.1 Introduction 115

5.2 Effect of hydrothermal treatment duration 115

5.2.1 Linear sweeping voltammetry （LSV） 116

5.2.2 Chronoamperometry 119

5.2.3 Electrochemical impedance spectroscopy 122

5.2.4 Mott-Schottky measurement (M-S) 124

5.3 Effect of hydrothermal treatment temperatures 129

5.3.1 Linear sweeping voltammetry 130

5.3.2 Chronoamperometry 132

5.3.3 Electrochemical impedance spectroscopy measurement (EIS) 133

5.3.4 Mott-Schottky measurement (M-S) 136

5.4 Summary 139

CHAPTER 6 CONCLUSIONS AND FUTURE WORKS 142

6.1 Conclusions 142

6.2 Future works 144

REFERENCES 146

LIST OF PUBLICATIONS

LIST OF TABLES

Page

Table 2.1 A summary of PC and PEC systems [51–56]. 15

Table 2.2 Variation in values of bandgap (E_g) of TiO_2 nanostructures 16

Table 2.3 Structural parameters, together with physical properties of three polymorphs of TiO_2 20

Table 2.4 Summary of PEC properties of the TiO_2 nanostructures 31

Table 2.5 Summary of photocatalytic (PC) water splitting using TiO_2 based nanostructures. 69

Table 2.6 Summary of photoelectrochemical (PEC) water splitting using TiO_2 based nanostructures 79

Table 3.1 Growth conditions of two sets of samples and the characterizations 81

Table 3.2 Detailed parameters used for the PEC measurements. 94

Table 4.1 Related structural parameters of samples at the (004) and (101) diffraction planes. 110

Table 5.1 Estimated equivalent circuit parameters. 123

Table 5.2 Estimated carrier lifetime and equivalent circuit parameters. 134

LIST OF FIGURES

Page

Figure 1.1 Comparison for finite and renewable planetary energy reserves (TW years) [5]. 1

Figure 1.2 Illumination of (a) Natural; (b) Artificial photosynthesis [5] 3

Figure 1.3 Number of publications against year (2014-2023) obtained from Web of science using the search terms 'PEC water splitting' or 'photoelectrochemical water splitting' (Topic) and filtered by Article (Document Type). Data collected on 8th March 2024. 4

Figure 2.1 Crystal structure of three different polymorphs: Anatase, Rutile and Brookite [16] 19

Figure 2.2 Band transition illustration: (a) allowed and (b) forbidden direct gap absorption of a photon with Eg energy (c) for the indirect gap, the assistance of a phonon is required [92] 22

Figure 2.3 Classification of nanostructures according to 0-D, 1-D, 2-D and 3-D [111] 26

Figure 2.4 Photogenerated charge transfer and light trapping in TiO2 photoelectrode with different nanoarchitectures, (a) powdered TiO2 photoanodes, (b) 1-D, (c) 2-D, and (d) 3-D building block units [115]. 28

Figure 2.5 Behaviour of photogenerated electrons and holes in anatase and rutile TiO2 powders, as revealed by time-resolved visible to mid-IR absorption spectroscopy [117] 29

Figure 2.6 Conventional electrochemical anodization setup [129] 34

Figure 2.7 Schematic diagram illustrating the idea of two-step anodization to improve the ordering of the grown nanotubes [138] 35

Figure 2.8 Synthesis of TiO2 nanotubes via template-assisted method [148] 36

Figure 2.9 Schematic of HR-CVD experimental setup [152] 37

Figure 2.10 Schematic diagrams for the transformation process of anatase TiO_2 from titanate [34] 42

Figure 2.11 Four distinct categories of TiO_2 nanostructured heterojunctions: (a) Schottky junction and (b) type-I, (c) type-II, and (d) type-III heterojunctions [194] 48

Figure 2.12 Schematic illustration of PEC cell (a) n-type Semiconductor photoanode and a metal cathode; (b) p-type Semiconductor photocathode and a metal anode [5]. 54

Figure 2.13 Band gap values (in eV) and band edge positions for selected semiconductors at pH=0 (vs NHE and the vacuum level as a reference) [216,217] 58

Figure 2.14 (a) Band diagram for a PEC cell based on a n-type semiconducting photoanode in the dark and (b) under irradiation [5]. 59

Figure 2.15 (a) Band diagram for a p-type semiconducting photocathode connected to a metal counter electrode in equilibrium in the dark and (b) under irradiation [5] 61

Figure 2.16 Effect of the applied bias, E, on the band bending in n-type semiconductors (a) $E > E_F$, (b) $E = E_F$, (c) $E < E_F$ [220] 61

Figure 2.17 Effect of the applied bias, E, on the band bending in p-type semiconductors (a) $E > E_F$, (b) $E = E_F$, (c) $E < E_F$ [220,221] 62

Figure 2.18 (a) High-angle annular darkfield scanning transmission electron microscopy (HAADF-STEM) and (b) STEM energy X-ray dispersive spectroscopy elemental maps of Ti (blue) and Ga (green) of 3.125 Ga-doped TiO_2; Photocatalytic stability of H_2 generation of 3.125% Ga-doped TiO2 (c) without and (d) with Pt co-catalyst (λ = 310–625 nm and T = 298 K) [224] 66

Figure 2.19 SEM images of the as-prepared samples: (a) TiO_2 nanotubes, (b) 2D MoS_2-modified black TiO_2 nanotubes (c) Photocatalytic HER performances of the samples [226] 66

Figure 2.20 (a) Schematic diagram illustrating the one-step photoinduced synthesis of Ag@Ni/TiO_2 photocatalysts (b, c)TEM, (d) HRTEM images of the Ag@Ni/TiO_2(1.5: 1.5) photocatalyst; (e) The photocatalytic H_2-production rate of various samples: (a) TiO_2, (d) Ag/TiO_2, (c) Ag@Ni/TiO_2(2.9:0.1), (d) Ag@Ni/TiO_2(2:1), (e) Ag@Ni/TiO_2(1.5:1.5), (f) Ag@Ni/TiO_2(1:2), (g) Ag@Ni/TiO_2(0.5:2.5) and (h) Ni/TiO_2; (e) Cycling runs for the photocatalytic H_2-evolution of Ag@Ni/TiO_2(1.5:1.5) photocatalyst [227]. 67

Figure 2.21 (a) TEM images of the as-synthesized S-TiO_2/S-RGO (0.2); (b) linear sweep voltammetry curves of the as-prepared photoanodes vs. Ag/AgCl under simulated sunlight (100 mW/cm^2) in 1 M KOH electrolyte [241] 72

Figure 2.22 (a) Schematic diagram depicting the synthesis of WO_{3-x}/TiO_2 nanorod arrays. (b) Linear sweep voltammetry curves (c) SEM images of WO_{3-x}/TiO_2 [242] 73

Figure 2.23 (a) Schematic synthesis procedure of core–shell structural TiO_2@Au_{25}/TiO_2 (TAT) nanowire arrays. SEM images of TAT-150C photoanode. (c d) Top view with different magnifications. (e) Cross-sectional view. (b) j–V curves measured at 1.23 V vs RHE of various TAT photoanodes [243]. 74

Figure 2.24 (a) Top SEM images of TiO_2 nanotube arrays obtained from a three-step electrochemical anodization (b) a HRTEM image in which a few Pd QDs deposited on the nanotube are clearly evident.(c) Photocurrent density generated by utilizing TiO_2 nanotubes and Pd@TNTA nanocomposites as photoanodes and Pt foil and Pd@TNTAs nanocomposites as cathodes in 0.5 M KOH in a photoelectrochemical (PEC) cell at a potential range of −1.1 to −0.9 V vs SCE, under 320 mW·cm−2 irradiation [125]. 74

Figure 2.25 (a) Schematic illustration of fabrication procedure of CdS/ZnO/TiO2composite films on FTO glass substrate (b) SEM

images of the top view section of TiO_2 array films and (C) CdS/ZnO/TiO_2 composite films [244] 76

Figure 2.26 Schematic description and corresponding SEM images of (a) branched nanorods TiO_2 photoelectrode. (b) Cross-sectional view and (c) top view. (d) PEC properties of the three types TiO_2 photoanodes.(e) IPCE spectra measured at an applied bias of 0.6 V versus RHE [36,112] 77

Figure 2.27 (a) Synthesis process (b) SEM image of NiFe-MOF/TiO_2 heterostructure (c) linear sweeping voltages (d) IPCE spectra of samples [248] 78

Figure 3.1 Flow chart of this work 82

Figure 3.2 Oven used in this work 83

Figure 3.3 (a) Annealing tube furnace (model Lenton VTF/12/60/700), and (b) a thermal tube furnace (schematic). 84

Figure 3.4 The diagram of the hydrothermal process 86

Figure 3.5 Schematic diagram of FE-SEM [263]. 88

Figure 3.6 Different emission types caused by interaction between incident 89

Figure 3.7 Schematic diagram of some components and angles of the goniometer HR-XRD [263] 91

Figure 3.8 Image of Agilent Technologies Cary 5000 UV-Vis-NIR spectrophotometer 92

Figure 3.9 Wavelength ranges of Carry 4000, Cary 5000 and Cary 6000i systems. 93

Figure 3.10 Image of Agilent Technologies Cary 5000 UV-Vis-NIR spectrophotometer 93

Figure 3.11 Photo image of the experimental setup and the schematic connection diagram for the PEC measurements 95

Figure 4.1 FESEM images of TiO_2 thin films under hydrothermal treatment for different durations (a) 2h (b) 4h (c) 6h (d) 12h (e) 24h and

insets are the magnification of image (a) (b) (c) (d), the cross-sectional view with a tilt of image (e) respectively. 97

Figure 4.2 Diameter distribution of nanowires in TiO_2-12h and TiO_2-24h. 98

Figure 4.3 Variation of O/Ti atomic ratio with the duration of hydrothermal treatment and inset EDX analysis of samples 100

Figure 4.4 XRD patterns for samples prepared at different hydrothermal treatment durations 101

Figure 4.5 (a) Diffuse-reflectance (b) Tauc plots of samples 102

Figure 4.6 Variation of Band gap with the hydrothermal treatment duration ... 103

Figure 4.7 FESEM images of TiO_2 films prepared at (a) 130 °C (b) 160 °C (c) 190 °C (d) 210°C and insets are the corresponding magnification images. 105

Figure 4.8 Variation of O/Ti atomic ratio with the temperature of hydrothermal treatment and inset displays EDX analysis of samples 107

Figure 4.9 Digital pictures of samples 107

Figure 4.10 XRD patterns for samples prepared in different hydrothermal treatment temperatures 108

Figure 4.11 Magnified XRD pattern for TiO_2-130 109

Figure 4.12 (a) Diffuse-reflectance (b) Tauc plots of samples 111

Figure 5.1 Linear Sweep Voltammetry (LSV) plots of samples prepared in different durations 116

Figure 5.2 Variation in maximum photocurrent density with the duration of hydrothermal treatment. 118

Figure 5.3 Transient response of the photocurrent versus time (I-t) 119

Figure 5.4 Rise and fall time of samples extracted from the I-t plots 120

Figure 5.5 Variation in ratio of I_{on}/I_{off} with the duration of hydrothermal treatment 121

Figure 5.6 The Nyquist plots (a) and bode-phase plots (b) for samples 122

Figure 5.7 Variation in carrier lifetime with the duration of hydrothermal treatment 124

Figure 5.8 Mott-Schottky plots for samples synthesized in different durations 125

Figure 5.9 Variation in carrier density with the duration of hydrothermal treatment 127

Figure 5.10 PEC water splitting mechanism in a PEC reaction cell with TiO_2 as photoanode 128

Figure 5.11 Linear Sweep Voltammetry (LSV) plots of samples 130

Figure 5.12 Variation of the maximum photocurrent density with the temperature of treatment 131

Figure 5.13 Transient response of the photocurrent versus time (I-t) of samples measured at 0.5V (vs. Ag/AgCl) 132

Figure 5.14 (a) Bode-phase plots (b) Electrochemical impedance spectroscopies of samples prepared in different temperatures 133

Figure 5.15 Mott-Schottky plots for samples synthesized in different temperatures 136

Figure 5.16 Variation in carrier density and width of space charge region with the temperature of hydrothermal treatment 138

Figure 5.17 Charge transfer mechanism on the interface of TiO_2 and the electrolyte 139

LIST OF SYMBOLS

$\mathring{A}$	Angstrom
α	Absorption coefficient
β	Full width at half maximum
ε	Dielectric constant
ε_0	Permittivity of vacuum
θ	Angle
λ	Wavelength
ι	Lifetime
η	Solar to hydrogen conversion efficiency
η_F	Faradic efficiency
C	Capacitance
C_S	Crystallite size
C_{sc}	Capacitance of space charge
C_{dl}	Double-layer capacitance
d	Interplanar spacing
e	Electron charge
ΔE^0	Standard potential of the electrochemical cell
E	Electron energy
E_F	Fermi level
E_g	Bandgap
E_{loss}	Inherent losses
f	Frequency
F	Faraday's constant
I_{max}	Maximum photocurrent
I_{on}	Photocurrent under illumination

I_{off}	Photocurrent without illumination
I_{sc}	Short circuit photocurrent
J	Photocurrent density
N_D	Carrier density
O_v	Oxygen vacancy
P	Pressure
P_λ	Intensity of the incident light
Pt	Platinum
P_{light}	Irradiance intensity
R_i	Resistance at the interfaces of electrodes
R_b	Bulk resistance of electrolyte
R_{H2}	Hydrogen generation rate
S	Entropy
T	Temperature
U	Internal energy
V	Volume
V_b	Applied bias
V_{FB}	Flat band potential
V_{oc}	Open circuit voltage
W_a	Warburg impedance
W	Width of space region
Z	Atoms per unit

LIST OF ABBREVIATIONS

0-D	Zero dimensional
1-D	1 dimensional
2-D	2 dimensional
3-D	3 dimensional
AAM	Anodic aluminium membranes
ABPE	Applied bias photon-to-chemical conversion efficiency
AC	Alternating current
ALD	Atomic layer deposition
AR	Analytical reagent
B-NRs	Branched nanorods
CB	Conduction band
CPE	Constant phase elements
CVD	Chemical vapor deposition
DMSO	Dimethyl sulfoxide
DI	Deionized
DMF	Dimethylformamide
EDX	Energy dispersive X-ray spectroscopy
EIS	Electrochemical impedance spectroscopy
FE	Faraday efficiency
FE-SEM	Field-emission scanning electron microscope
FTO	F-doped Tin Oxide
HAADF-STEM	High-angle annular darkfield scanning transmission electron microscopy
HER	H_2 evolution reaction
HRTEM	High-resolution transmission electron microscopy
HR-XRD	High-resolution X-ray diffraction
ITO	Indium Tin Oxide
IPCE	Incident photon to current efficiency
LED	Ligh-emitting diode
LDH	Layered double hydroxide
LSV	Linear sweeping voltammetry
MOF	Metal organic framework

MS	Mott-Schottky
NA	Not available
NHE	Normal hydrogen electrode
NPs	Nanoparticles
NRs	Nanorods
NTAs	Nanotube arrays
OER	O_2 evolution reaction
PEC	Photoelectrochemical
PC	Photocatalytic
PLD	Pulsed laser deposition
PV	photovoltaic
QDs	Quantum dots
SC	Space charge
SCE	Saturated calomel electrode
SILAR	Successive ionic layer adsorption and reaction
SPR	Surface plasmon resonance
STH	Solar to hydrogen
UV	Ultraviolet
VB	Valence band
XL	Xenon lamp

SIFAT FOTOELEKTROKIMIA STRUKTUR NANO TITANIUM DIOKSIDA YANG DITUMBUHKAN OLEH TEKNIK HIDROTERMA

ABSTRAK

Pemisahan air fotoelektrokimia (PEC) adalah teknik yang sangat menggalakkan untuk menukar tenaga suria kepada tenaga kimia dengan menyimpan tenaga dalam bentuk ikatan kimia akibat hasil (H_2 dan O_2). Selain itu, bahan api H2 sangat menarik untuk memenuhi keperluan penggunaan tenaga yang semakin meningkat. Dalam kerja ini, struktur nano TiO_2 bukan stoikiometrik anatase yang diubah daripada titanat telah disediakan oleh teknik hidroterma alkali pada tempoh rawatan yang berbeza (4j-24j) dan suhu (130°C-210 ° C). Morfologi sampel telah dicirikan oleh mikroskop elektron pengimbasan pelepasan medan (FESEM) dan menunjukkan bahawa perubahan morfologi TiO_2 daripada lembaran nano kepada wayar nano. Juga, nisbah atom O/Ti yang diekstrak daripada spektrum EDX menunjukkan bahawa semua sampel secara tidak langsung telah menunjukkan struktur bukan stoikiometri dengan formula boleh dikemukakan sebagai TiO_{2-x} kerana kekurangan oksigen. Fasa struktur nano TiO_2 disahkan sebagai anatase oleh corak pembelauan sinar-X (XRD). Sifat optik sampel diukur dengan pengukuran UV-vis-NIR dan mencadangkan bahawa tempoh masa yang lama dan suhu tinggi rawatan hidroterma kedua-duanya menyebabkan peningkatan dalam pantulan meresap. Berkenaan dengan sifat PEC, sel tindak balas tiga elektrod yang diperbuat daripada fotoanod TiO_2, wayar platinum dan elektrod rujukan Ag/AgCl digunakan untuk menilai prestasi sampel. Antara set sampel pertama yang disediakan dalam tempoh yang berbeza, empat jam sintesis hidroterma TiO_2 yang disepuhlindapkan dalam udara pada 500°C selama 90 minit menunjukkan tindak balas arus foto

optimum dengan ketumpatan arus foto maksimum 149.1μA/cm^2 pada 0.8 V berbanding Ag/AgCl. Dalam set kedua sampel yang disediakan dalam suhu yang berbeza, TiO_2 yang disediakan pada 130°C rawatan hidroterma yang sepuhlindap dalam udara pada 500°C selama 90 minit menunjukkan prestasi PEC yang optimum dengan ketumpatan arus foto tertinggi 265μA/cm^2 pada 1 V (vs. Ag/AgCl). Kedua-dua sampel unggul berkongsi beberapa ciri biasa, seperti ketumpatan pembawa yang dipertingkatkan, jangka hayat pembawa yang panjang dan kawasan caj ruang sempit. Di samping itu, kedua-dua sampel ini menunjukkan morfologi lembaran nano dengan luas permukaan yang besar yang memberi manfaat kepada penangkapan cahaya dan seterusnya meningkatkan pengujaan pembawa. Secara ringkasnya, tempoh rawatan yang agak singkat dan suhu rawatan yang rendah memberi manfaat kepada sifat PEC. Selain itu, morfologi lembaran nano didapati lebih unggul daripada morfologi wayar nano berkenaan dengan sifat optik dan PEC. Oleh itu, struktur nano TiO_2 ini diubah daripada titanat menggunakan kerajang Ti sebagai prekursor boleh digunakan dengan sewajarnya untuk aplikasi PEC dan pengubahsuaian boleh dilakukan untuk prestasi pemisahan air yang lebih baik.

PHOTOELECTROCHEMICAL PROPERTIES OF TITANIUM DIOXIDE NANOSTRUCTURES GROWN BY HYDROTHERMAL TECHNIQUE

ABSTRACT

Photoelectrochemical (PEC) water splitting is a highly promising technique to convert solar energy into chemical energy by storing energy in the form of chemical bonds of the reaction products (H_2 and O_2). Additionally, H_2 fuel is of great interest to meet the requirement of increasing energy consumption. In this work, anatase non-stoichiometric TiO_2 nanostructures transformed from titanates were prepared by the alkaline hydrothermal technique at different treatment durations (4h-24h) and temperatures (130°C-210°C). The morphologies of samples were characterized by field emission scanning electron microscopy (FESEM) and demonstrated that the morphological change of TiO_2 from nanosheets to nanowires. Also, the O/Ti atomic ratio extracted from the EDX data indicates that all the samples have indirectly shown non-stoichiometric structures with the formula can be presented as TiO_{2-x} because of the oxygen deficiency. The phase of TiO_2 nanostructures is confirmed to be anatase by X-ray diffraction (XRD) patterns. The optical properties of samples were measured by UV–vis-NIR measurement and suggested that long-time duration and high temperature of hydrothermal treatment both caused the increase in the diffuse reflection. With respect to the PEC properties, a three-electrode reaction cell made of TiO_2 photoanode, platinum wire and Ag/AgCl reference electrode was used to evaluate the performance of samples. Among the first set of samples prepared in different durations, TiO_2 with hydrothermal treatment of four hours, annealed in air at 500°C for 90 min showed the optimal photocurrent

response with the maximum photocurrent density of 149.1μA/cm^2 at 0.8 V vs. Ag/AgCl. In the second set of samples prepared in different temperatures of hydrothermal treatment, the TiO_2 prepared at 130°C of hydrothermal treatment annealed in air at 500°C for 90 min displayed the optimum PEC performance with the highest photocurrent density of 265μA/cm^2 at 1 V (vs. Ag/AgCl). The two superior samples share some common features, such as improved carrier density, long lifetime of carriers, and narrow space charge region. In addition, these two samples both show nanosheet morphology with big surface area which is of benefit to the light capturing and furthermore enhancing the excitation of carriers. In short, relatively short treatment duration (2-6h) and low treatment temperature are beneficial to PEC properties. Besides, nanosheet morphology is found to be more superior than nanowire morphology regarding to optical and PEC properties. Thus, these TiO_2 nanostructures transformed from titanates using Ti foils as precursors could be appropriately used for PEC application and the modification can be done for better water splitting performance.

CHAPTER 1

INTRODUCTION

1.1 Introduction

Energy consumption is essential to our modern civilization and present economic development. But the constant increasing demand forces human beings to explore and utilize much more energy sources which seriously affects the climate and causes social conflict in global policies. The current rate of global energy consumption is about 18.5 TW furthermore, is predicted to be 30 TW by 2050 and almost 50 TW by the end of 21st century [1–3]. Up to now, the fossil fuel makes the most contribution to the global sources of power. The large amount utilization of fossil fuels has induced high emissions of greenhouse gases such as CO_2, and the emission will grow followed by the increase of population [4]. Thus, developing a sustainable energy source to gradually replace the fossil fuels and mitigate the greenhouse effect is an urgent mission for human beings.

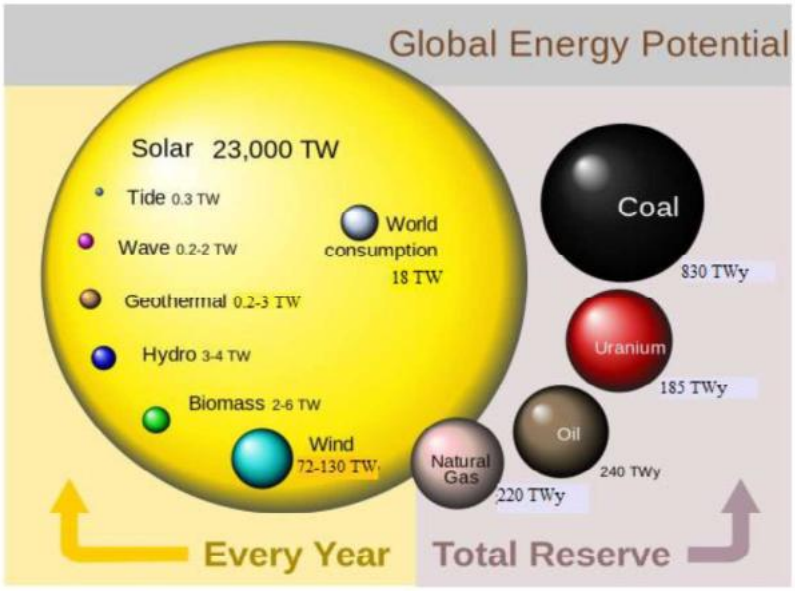

Figure 1.1 Comparison for finite and renewable planetary energy reserves (TW years) [5].

Figure 1.1 shows several potential renewable energy sources such as hydropower, biomass, geothermal, waves, tides, wind, solar etc. Among them, the solar energy stands out due to its vast energy reserves. Besides, the wind energy is also an appropriate alternative considering the quantity of the energy reserve every year. However, most of the energy reserves listed on the Figure 1.1 are derived from or depend on solar energy either directly or indirectly. These are referred to as first-order (e.g., biomass) and second-order (e.g., fossil fuels formed from ancient biomass) by-products of solar energy, meaning that they cannot stand alone to meet the energy requirement of the world consumption. Thus, solar energy as a clean and inexhaustible energy source is a promising candidate.

Every year, the sun irradiating the Earth is approximately 5.0×10^{12} terajoules (TJ) [6], which is enough to support the human annual energy consumption, approximately 5.67×10^{8} TJ, if the irradiation is efficiently used [3]. Solar energy can be harnessed and transformed into various forms of energy for practical applications: thermal energy through photothermal processes, electrical energy through photovoltaic mechanisms, and chemical energy stored in chemical bonds of the products via photocatalytic reactions [7]. The photothermal processes are related to the conversion of solar energy to heat and then stored in a thermal reservoir such as H_2O or dry rocks. Furthermore, the heat energy also can transform into mechanical and/or electrical energy (e.g., a steam turbine for the creation of electricity) [7]. In the photovoltaic process, solar energy can be converted to electricity through semiconductor materials under irradiation. Generally, the solar cells of photovoltaic (PV) are made of p-n junctions, and the electron-hole pairs will be generated in the p-n junctions under solar radiation [8]. With the applied bias, the electrons transfer from n- to p-side semiconductor resulting in the electric current [9].

In the photocatalytic process, solar energy is harnessed and converted into chemical energy, stored in the form of products like hydrogen (H_2) and oxygen (O_2), through reactions occurring on the catalyst surface [10].

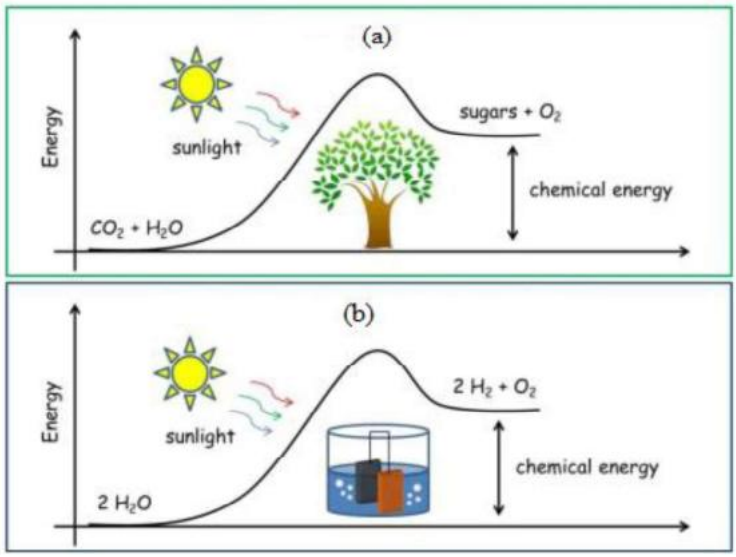

Figure 1.2 Illumination of (a) Natural; (b) Artificial photosynthesis [5]

Photosynthesis in nature enables plants to harness solar energy, converting CO_2 and H_2O into hydrocarbons and oxygen (O_2). Photoelectrochemical water splitting also can generate H_2 and O_2 from H_2O through conversion of solar energy, which is called artificial photosynthesis (Figure 1.2). Herein, the H_2 fuel as a clean energy source is eagerly anticipated to replace fossil fuels to provide the most energy for the development since the only byproduct of the reaction is H_2O. Moreover, abundant water in the world also can ensure large number of precursors that can be easily obtained for the artificial photosynthesis. The photocatalysts used for water splitting include, but not limited to, TiO_2, ZnO, Fe_2O_3, WO_3, and $BiVO_4$ [11][12]. The water splitting can be achieved through photocatalytic (PC) and photoelectrochemical (PEC) processes [13]. Different from the photocatalytic method, the latter method is implemented with the applied bias which can provide

more energy for the reaction and also does a great favour to the gas separation by generating O_2 and H_2 on different electrodes. Photoelectrochemical water splitting using solar energy has been considered as a quite competitive and promising option for the industry sectors [3].

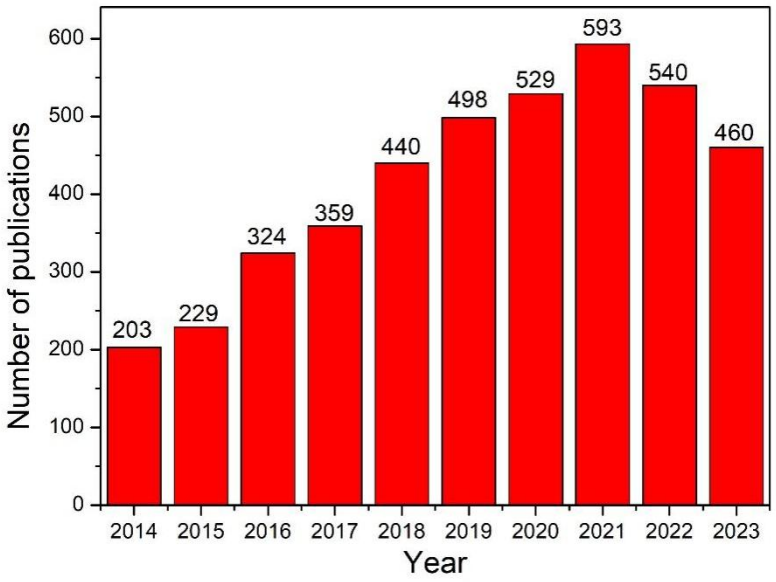

Figure 1.3 Number of publications against year (2014-2023) obtained from Web of science using the search terms 'PEC water splitting' or 'photoelectrochemical water splitting' (Topic) and filtered by Article (Document Type). Data collected on 8th March 2024.

Since 1972, Fujishima and Honda reported the PEC water splitting using TiO_2 as the photoanode, a significant number of related studies have emerged. The number of publication against the year is shown in Figure 1.3 [14]. The photoelectrochemical cells used for the water splitting are always contain three electrodes: TiO_2 photoanode, Pt counter electrode and reference electrode. TiO_2, a n-type semiconductor, shows thermodynamic stability and its band edges not only meet the position requirement of the water splitting, but also prevent itself from the self-oxidizing by the holes in the valence band [11,12,15]. Generally, there are three different phases for TiO_2 existing in the nature: anatase, rutile, and brookite [16].

Among them, the brookite is unstable and barely be obtained in the laboratory, while the other phase is relatively stable and easily synthesized for research. The energy gap of anatase is 3.2 eV, whereas that of rutile is measured at 3.0 eV. There are several methods used for the synthesis of TiO_2 nanostructures, like anodization [17,18], chemical vapor deposition [19,20], hydrothermal [21–23], sputtering [24,25] and so on.

Hydrothermal method is broadly used to prepare TiO_2 due to its facile procedure and high production rate, and generally can be classified into two categories: acid-hydrothermal and alkaline-hydrothermal methods [26]. In acid-hydrothermal method, the titanium salts (titanium butoxide, titanium tetraisopropoxide) or $TiCl_4$ as the titanium source are always mixed with inorganic acid (HCl) to obtain the TiO_2 nanorod [27–30]. In alkali-hydrothermal approach, the TiO_2 nanoparticles react with the alkaline solution (NaOH) to get the nanotube or nanowire product [31,32]. These two different approaches have different mechanisms, and the final products also correspond to different morphologies and phases. The reaction between TiO_2 nanoparticles and NaOH solution in the alkaline hydrothermal method to get TiO_2 nanostructures can be divided into three stages: formation of sodium titanates in the alkaline aqueous, ion exchange to obtain hydrogen titanates, annealing process for the final TiO_2 nanostructure products [13,33,34]. The TiO_2 nanostructures transformed from the titanates are proved to be an excellent photocatalyst in the photocatalytic water splitting.

However, the drawbacks like fast recombination of electron/hole pairs and low mobility of carriers still limits the performance of TiO_2 in the photocatalytic water splitting. Additionally, the final products H_2 and O_2 gases cannot be separated

immediately during water splitting process [13]. Consequently, photoelectrochemical water splitting with extra power provided by applied bias for improved charge separation and transport attracts much attention. Thus, some researchers tried to use Ti foils as the precursors to form TiO_2 films on the Ti foils that can be directly employed as electrodes. Comparing to the TiO_2 powders, the TiO_2 films grown on Ti foils are very suitable to be the photoelectrodes without any modifications. So, the physical properties of the TiO_2 films on Ti foils transformed from titanates require to be thoroughly investigated with the influence from the hydrothermal treatment. Moreover, the reports about the photoelectrochemical properties of the TiO_2 films transformed from titanates are few, and the limited studies only concern the photo response. The detailed photoelectrochemical properties related to the photoelectrochemical water splitting have not been investigated.

1.2 Motivation and Problem Statement

Water splitting for obtaining H_2 fuel is a promising method to mitigate the coming energy crisis in the future through solar energy conversion process. Solar energy as a renewable energy source is much more of interest due to its inexhaustible supply, universality, high capacity, and environmental friendliness. Water splitting can alleviate the environmental pollution caused by the combustion of fossil fuels since the resultant product H_2 is a promising alternative source energy. Besides, large amount of NaOH waste requires to be decomposed every year from the industry. Nevertheless, the photo-to- current conversion efficiency is around 5-12% and the commercialization for continuous H_2 production needs further advancement to demonstrate the practicality of PEC devices [12,13]. For the water splitting process, wide bandgap (3.0 eV) limits the light absorption to the ultraviolet (UV) light region,

which is only taken up 3-5% of solar light. Additionally, the low efficiency in the carrier separation results in high carrier recombination.

With regard to TiO_2 nanostructure, it as a n-type semiconductor is broadly used as the photocatalyst for the water splitting. There are many methods can be used for the synthesis of TiO_2, namely anodization, sol-gel, hydrothermal and template method. Among the synthesis methods, the hydrothermal technique is the most widely used in industry for large scale production. Unfortunately, long reaction duration and high temperature are required in the hydrothermal treatments to ensure the quality of the product. Specifically, duration around 10h and temperature above 150°C are always employed in the previous works [35]. However, the high temperature and long duration may result in deformation in the structure due to the dissolution of the intermediate titanates in the hydrothermal treatment. Therefore, shortening the hydrothermal treatment duration, lowering the treatment temperature are a worthy attempt to save the energy and meanwhile simplify the procedure of TiO_2 synthesis using hydrothermal method.

In the alkaline hydrothermal method, TiO_2 nanoparticles are always used as the precursors to fabricate the TiO_2 nanotubes in powdered form, which are difficult to collect after every experiment. In the water splitting process using TiO_2 powders as photocatalysts, the immediate separation of H_2 and O_2 gases produced is not possible. and the right removal of the TiO_2 powder is challenging, as it is essential to avoid reaching a photo stationary state, where the rates of photocatalytic reactions reach equilibrium, halting further progress. Additionally, the powder-form TiO_2 must be assembled in a film or be screen printed on one conductive substrate to be the photoelectrode for PEC water splitting [28,36–39]. Thus, comparing to the powder

form, the TiO_2 films are convenient in utilization. To do a modification, some researchers tried to use the Ti foils instead of the TiO_2 particles as the precursors and substrates in the alkaline hydrothermal method to prepare TiO_2 films [34,40]. These TiO_2 nanostructure films with Ti foils as the conductive substrates are more suitable to be photoelectrodes for the photoelectrochemical reaction cells. But literatures reported about the TiO_2 films prepared by alkaline hydrothermal method are few and the properties of this TiO_2 structure are not unravelled. The optimized synthesis conductions and the influence of the hydrothermal treatment should be explored.

The works focusing on the hydrothermal method to prepare TiO_2 nanostructures ever reported the growth mechanism of TiO_2. In this process, sodium titanates as the resultant product of TiO_2 particles and NaOH solution are firstly formed in the hydrothermal treatment, and then, through ion exchange process in the acid post washing process hydrogen titanates are obtained. At last, TiO_2 nanostructures are available after calcination [12,13]. The powder form of those TiO_2 transformed from titanates limits the study to the growth mechanism, morphology changes, phase compositions, and photocatalytic applications [22,41–45]. The TiO_2 powders prepared by the hydrothermal method are not suitable to be the photoelectrodes for PEC water splitting. For PEC properties investigation, an extra process like screen printing or doctor blade is needed to cast powder TiO_2 on conductive substrate. These techniques are complex since the paste should be prepared in advance and multiple deposition times are needed [46]. Besides, there are bound to be particle losses in the washout or displacement process, and high viscosity requirement, low volatility, particle accumulation at high concentration of slurry/paste are also their limitations [47,48]. Thus, a modification should be done to

prepare TiO_2 film through alkaline hydrothermal method for the PEC-property study of TiO_2 transformed from titanates.

TiO_2 nanowire, nanosheet and nanotube, as the mainstream morphologies, are commonly used in the PEC water splitting. From literatures, nanosheet is of much more interest due to its large light-harvesting ability caused by the high surface to volume ratio [10,11]. Also, the nanosheet has a high photocatalytic activity attributed to the large surface area, reduced charge recombination, short charge transport pathways, and enhanced light absorption [49][50] . Therefore, the nanosheet TiO_2 is worthy further investigation. However, the facile synthesis method of TiO_2 nanosheet is lacking which limit the widely study of the nanosheet morphology.

From above, the problem statements can be summarized as below:

i. Further exploration is needed to optimize and understand the formation of high-performance TiO_2 structures using Ti foil as a precursor for PEC water splitting,

ii. For PEC property investigations, techniques like doctor blading and screen printing are commonly used to cast powder TiO_2 on conductive substrates, but challenges such as particle losses, viscosity control, and slurry stability still impact the reproducibility and scalability of these processes.

iii. Approaches that enable the controlled and reproducible fabrication of high-quality nanosheet films suitable for in-depth photoelectrochemical investigations remain underexplored.

1.3 Research Objectives

The aim of this work is to fabricate and evaluate the photoelectrochemical properties of the TiO_2 nanostructure films with the following specific objectives:

i. Explore the effect of hydrothermal treatment (duration and temperature) on the structural and morphological properties of TiO_2 synthesized from Ti foil for PEC water splitting

ii. To conduct a systematic study of PEC properties of TiO_2 nanostructures transformed from the titanates especially the influence of hydrothermal treatment duration and temperature on the photocurrent density, carrier lifetime, and carrier density.

iii. To investigate the PEC properties of nanosheet grown under different conditions.

1.4 Research Contribution

The contributions of this work are listed as below:

1. TiO_2 nanostructures (nanosheets and nanowires) films transformed from titanates were successfully synthesized by facile alkaline hydrothermal method using Ti foils as both precursors and conductive substrates with different durations (2h-24h) and temperatures (130°C-210°C).

2. The enhanced PEC performance of the TiO_2 photoelectrode was because of the large surface of nanosheet, long lifetime discovered by Electrochemical Impedance Spectroscopy measurement, narrower space charge region and increased carrier concentration as revealed by Mott-Schottky analysis.

3. The effect of morphological changes on the PEC performance emerging from the influence of hydrothermal treatment has been investigated.

1.5 Thesis Outline

In this project, two sets of the TiO_2 films on Ti foils are fabricated by alkali-hydrothermal method at different hydrothermal treatment durations and temperatures, followed by the studies on the morphological, optical, and structural properties. The photoelectrochemical properties as the key section were paid a lot of attentions. The photocurrent density was measured by the linear sweeping voltammetry (LSV) to show the change of photocurrent density under the applied bias. The photo response was evaluated by the chronoamperometry to present the difference of photocurrent caused by the illumination. Then the electrochemical impedance spectroscopy (EIS) measurement was employed to give a further insight of the carrier transfer process with respect to the charge transfer resistance and the carrier lifetime. The Mott-Schottky (M-S) analysis was done for the carrier density and also can offer the information for the band position.

Chapter 1 gives a brief background of the fossil energy consumption and the solar energy as a promising energy source to be used by PEC technology. The properties of TiO_2 and the fabrication methods are also introduced as well as the potential of it to be photocatalyst for PEC water splitting. The problem statement, motivation, objectives and originality of this work are also exhibited in this chapter.

Chapter 2 introduces the research background and literature review on the TiO_2 as a photocatalyst for water splitting. The history, growth techniques and modification methods of TiO_2 are also detailed. Besides, the mechanism of PEC water splitting, the requirement of the photoelectrode and the interfacial charge

transfer process are presented. The chapter also summarizes the previous works on TiO_2 for photocatalytic and photoelectrochemical water splitting for H_2 generation at the last.

Chapter 3 focuses on the methodology, setup, experimental works in this research. The synthesis process is explained step by step for two sets of samples including hydrothermal treatment, acid washing, and calcination. The growth mechanism of the TiO_2 prepared by alkaline hydrothermal method is illustrated along with the influence of different procedures. Moreover, the characterization techniques are introduced about the working principles.

Chapter 4 presents the results of the two sets of TiO_2 samples prepared under different durations and temperatures, respectively. The morphologies are uncovered by the Field-Emission Scanning Electron Microscope (FESEM), the structural properties were assessed by the X-Ray diffraction technique, and the optical properties are evaluated by the UV-Vis-NIR spectrophotometer. Based on the data, the influence of hydrothermal temperatures and durations on the morphological, optical and structural properties are further discussed.

Chapter 5 encompasses the PEC performance of the TiO_2 films as photoelectrodes in PEC cell. The photocurrent density is measured in different voltage and the difference of photocurrent caused by the illumination is evaluated by the chronoamperometry measurement. The charge transfer process, band structure, and carrier density are deduced by Electrochemical impedance spectroscopy and Mott-Schottky analysis.

Chapter 6 concludes of the results and provides recommendations for further works regarding the TiO_2 nanomaterial for H_2 generation.

CHAPTER 2

BACKGROUND AND LITERATURE REVIEW

2.1 Introduction

This chapter provides the basic background of TiO_2 semiconductor, water splitting mechanism and related literature review for water splitting using TiO_2 electrode. TiO_2 as the material used for water splitting are detailed illustrated with its polymorphs, structural, optical, and electronic properties. In addition, several fabrication methods namely anodization, template, chemical vapor deposition, sol-gel and hydrothermal technique are introduced. Besides, modifications in TiO_2 for improved physical properties like metal and nonmetal doping, heterojunction, and other treatment are elaborate. Following the detailed introduction of TiO_2 material, the hydrogen production as the final application as well as the recent development of photocatalytic and photoelectrochemical water splitting using TiO_2 electrode as reported in literature are also summarized and reviewed. Table 2.1 is a summary of the photocatalytic and photoelectrochemical system.

Table 2.1 A summary of PC and PEC systems [51–56].

Experimental details	PC water splitting	PEC water splitting
Catalysts form	Powder (majority)	Thin films
Incident light	All directions	Vertical direction on the catalyst films
Energy input	Solar energy	Solar energy and external electricity
Gases collecting	Separating process required	Directed collected from separated electrodes
Efficiency benchmarks	η	η/ IPCE/ others
Efficiency	Below 5%	0.5%-12%
Recycle of catalysts	Complex and time consuming	Simple and effective

2.2 Titanium dioxide

Titanium dioxide (TiO_2), a IV–VI metal oxide, is the naturally existing oxide of titanium and also is a white pigment can be used in making inks, plastics, toothpaste, sunscreen, and cosmetic products. It has attracted substantial attention as an inorganic material, due to its versatile advantages such as inexpensiveness, nontoxicity, stability, natural abundance and excellent photocatalytic activity [57,58]. As a photocatalyst, it can be used for diverse applications namely water purification [59], gas sensing [36,37], dye-sensitized solar cells [21,60], photodetectors [41,61], and degradation of pollutants [62,63].

2.2.1 History of Titanium dioxide

Table 2.2 Variation in values of bandgap (E_g) of TiO_2 nanostructures

Morphology	Preparation method	Substrate	Growth parameters	Phase	E_g(eV)	Ref.
TiO_2 nanotube	anodization	Ti foil	anodization for 2 h, annealing at 850 °C via a stream of water vapour/N_2 gas for 3h	rutile	3.09	[37]
TiO_2 nanorod	hydrothermal	FTO	hydrothermal treatment at 180 °C for 6 h, annealing at 500 °C	rutile	3.18eV	[64]
TiO_2 nanorod	oblique-angle deposition	ITO	growth rate at 0.3 nm/s, annealing at 550°C for 2 h in air.	anatase	3.27eV	[65]
TiO_2 nanowire	hydrothermal	Ti foil	hydrothermal treatment at 210°C for 6h, annealing in air at 500°C for 90 min	anatase	3.29eV	[66]
TiO_2 nanotube	anodization	Ti foil	Anodization at 60V for 2 h, annealing at 650 °C for 2h	rutile	3.39eV	[67]
TiO_2 nanotube	hydrothermal	Ti foil	Annealing at 850°C under a manageable stream of water vapor/nitrogen in a tube furnace for 3 h	rutile	3.14 eV	[61]
TiO_2 film	hydrothermal	Ti foil	hydrothermal treatment at 150 ◦C for 2h, annealing in air at 500 °C for 90 min	anatase	3.22eV	[68]

As early as in the 1960s, the photoinduced phenomena of the semiconducting solids such as TiO_2 and ZnO under UV light irradiation were investigated by researchers [69,70]. The band theory of semiconductors has provided an explanation for these observations, which is now widely accepted. Some molecules, such as O_2 and H_2O, were observed can be adsorbed on or desorbed from the solid semiconductor surfaces under UV irradiation [71,72]. In 1972, TiO_2 was used for water photolysis by Fujishima and Honda, since then much more effort was put into this material to

explore its full potential on photocatalytic applications [14]. The investigation of S. Frank and A. Bard in 1977 provided an insight into the photocatalytic oxidation of aqueous sulphite and cyanide ions, which triggered the incorporation of TiO_2 in photocatalytic water purification [73]. This led to the formulation of the mechanistic notion that, the photogenerated electrons in TiO_2 move to the Pt metal to induce reduction reactions, while photogenerated holes remain in the valence band of TiO_2 and migrate to its surface for oxidation reactions [74]. Therefore, the charge separation of photogenerated electrons and holes is beyond doubt the most important process in photocatalysis process employing semiconductors, that is, the so-called photoelectrochemical mechanism. Subsequently, TiO_2 antifogging applications were discovered by Wang et al. in 1999 through the contact angle and X-ray photoelectron spectroscopy method [75].

Early studies mainly focused on zero dimensional TiO_2 nanoparticles because of the large surface area and a broadened band gap [76]. However, the unavoidable disadvantages brought by the structural disarrays and large grain boundaries, such as low charge-carriers mobility, high charge-carriers recombination rate and high recycling cost limit the utilization of it [77,78]. Recently, one dimensional (1D) nanostructure has been extensively studied including nanorod, nanotube, nanowire and nanofiber. Generally, the diameter of a 1D nanostructure is ranging from 1 to 100 nm. Therefore, 1D TiO_2 nanostructured materials display a relatively large specific surface area which is favourable to photogenerated carriers to transfer along the axial direction [79]. But the wide band gap of TiO_2 (anatase: 3.2 eV, rutile: 3.0 eV) makes it can only absorb UV light, which is only taken up 3-5% of solar light, the large amount of visible light is wasted due to their low photon energy. The bandgaps of TiO_2 fabricated by different methods are shown in Table 2.2, from which it can be observed

that the lowest value of bandgap is 3.09eV. Since initial synthesis of TiO_2 nanotubes utilising the template-assisted approach by Hoyer, the effects of doping strategies, manufacturing variables, and applications have grown exponentially [47,48].

2.2.2 Titanium dioxide polymorphs

TiO_2 (titania) is a transition metal oxide and offers three important polymorphs in nature: anatase, rutile, and brookite and the crystal structure of the polymorphs are shown in Figure 2.1 [79]. The composition for each TiO_2 phase is the same, but each phase corresponds to a different crystal structure due to the different arrangement of atoms, and also results in different physical and chemical properties. Many factors can impact the phases of crystal in the synthesis process, such as fabrication method, temperature of thermal treatment, pH, and duration etc [80]. Among the three polymorphs in bulk form, anatase and brookite are metastable phases, while rutile is stable phase with the lowest free energy under normal condition. The two metastable phases can transform irreversibly to the stable rutile phase at an elevated temperature. But for nanomaterials with the crystallite sizes smaller than ~10-30 nm, anatase phase is the most stable one [56]. The brookite is generally prepared by hydrothermal method with a more open framework structure, and a larger specific capacity than other phases. In 1916, Vegard performed the structural investigation of rutile and anatase using ionization method [81], while the crystal structure of brookite was first demonstrated by Pauling and Sturdivant through powder X-ray diffraction (XRD)method in 1928 [82]. Later In 1955, the crystal structures of anatase and rutile were amended by Cromer and Herrington using XRD method as well [83].

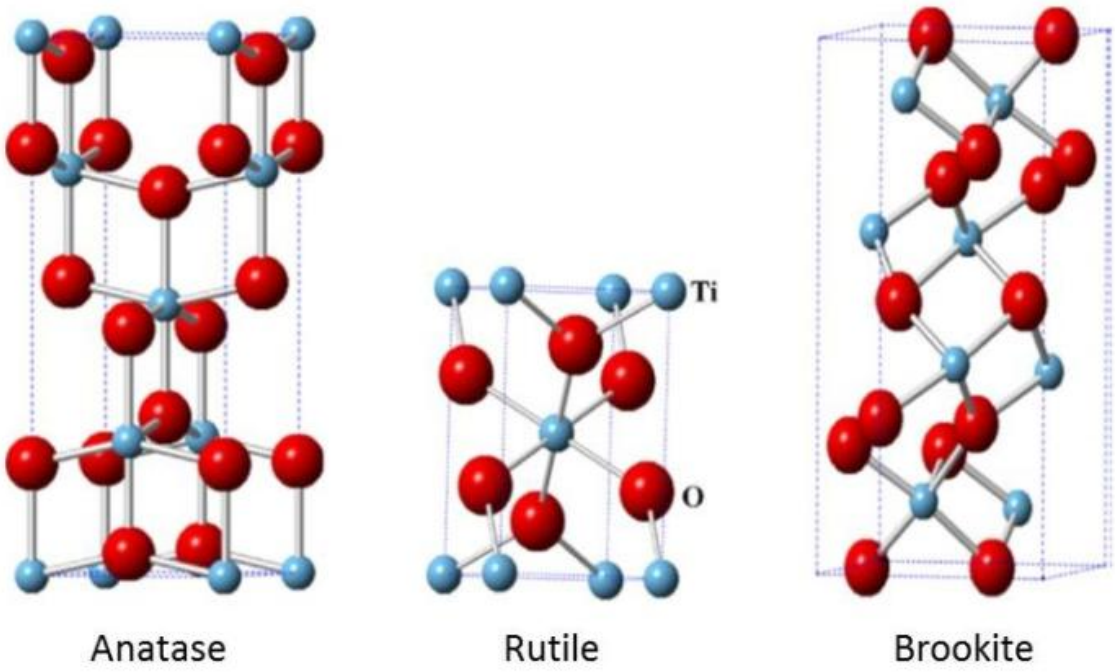

Figure 2.1 Crystal structure of three different polymorphs: Anatase, Rutile and Brookite [16]

2.2.3 Structural properties of titanium dioxide

In titania forms, titanium cations (Ti^{4+}) are coordinated to six oxygen anions (O^{2-}), forming distorted TiO_6 octahedra. The octahedra in anatase and rutile only share edges at (001) planes, whereas both edges and corners are shared (Figure 2.1) in brookite. The octahedron chains are arranged in zigzag for anatase phase while in linear form for rutile TiO_2. Thus, the anatase TiO_2 has a lower density and larger specific surface area than that of rutile TiO_2. Besides, both crystalline anatase and rutile are of tetragonal structure with lattice parameters: a = b =0.3784 nm, c = 0.9515 nm (anatase), and a = b = 0.4593 nm and c = 0.2958 nm (rutile), respectively. While Brookite has an orthorhombic structure with a=0.915 nm, b=0.544 nm, and c=0.514 nm. In lab-created materials and many other titania-based device applications, anatase and rutile are more common than brookite [84]. Table 2.3 presents the structural parameters, physical and mechanical properties of three different phases of TiO_2.

Table 2.3 Structural parameters, together with physical properties of three polymorphs of TiO_2

Polymorphs	Anatase	Rutile	Brookite	Ref.
Crystal system	Tetragonal	Tetragonal	Orthorhombic	[85]
Space group	I41/amd	P42/mnm	P b c a	[85]
Atoms per cell (Z)	4	2	8	[85]
Lattice parameters (25°C)	a = b =0.3784 nm, c = 0.9515 nm	a = b = 0.4593 nm c = 0.2958nm	a=0.9174nm b=0.5439nm c=0.5163nm	[85]
Density (25°C) (kg/m^3)	3894	4130	4250	[85]
Molecular weight (g/mol)	79.88	79.9	79.866	[85]
Optical band gap (eV)	3.20	3.00	3.35	[85]
Refractive index	2.52	2.9 or 2.75	2.63	[85]
Resistivity (Ωcm)(25°C)	10^5	10^{12}	10^5	[85]
Dielectric constants	31	173	NA	[85]
Conductivity (25°C) (1/Ωcm)	10^4–10^7	10^4–10^7	NA	[85]
Melting point (°C)	Transformation to rutile	1825	Transformation to rutile	[85]
Thermal expansion coefficients (TECs) $\times 10^{-5}$ (°C−1) at 900°C	linear (α_a): 0.53 linear (α_c): 1.04 volumetric(β): 2.17	linear (α_a): 0.87 linear (α_c): 1.01 volumetric(β):2.83	linear (α_a): 0.68 linear (α_b): 0.69 linear (α_c): 1.05 volumetric(β):2.40	[85]

Electron effective mass	~20m_e	0.4-1m_e	NA	[86]
Carrier mobility(cm^2/v/s)	~1-10	~0.1-0.3	NA	[86]

2.2.4 Optical properties of titanium dioxide

Generally, the optical phenomena like absorption, reflectance, transmission, diffraction and scattering are related to the interaction with electromagnetic (EM) radiation. In semiconductors, the chemical bonding, atomic structures and electronic band are the factors to determine the optical properties of the material [87]. For TiO_2, its optical properties primarily fall within the ultraviolet and visible light range. However, as ultraviolet light accounts for only 3–5% of the solar spectrum, various modifications, including doping, heterojunction formation, and hydrogenation, have been implemented to extend the absorption of TiO_2 into the visible light region. Hereby, the colour change of the TiO_2 is a distinct signal of the change of light absorption ability. It has been reported that the white coloured TiO_2 changed to yellow, black, brown as the N, C, P, was doped into the structure. Furthermore, with the concentration of doped B rising from 2 to 10 wt%, the colour of TiO_2 became brown, grey and green [88–91].

In the semiconductor, the conduction band (CB) is the energy level where electrons are free to move and conduct electricity, while the valence band (VB) is the highest range of energy levels where electrons remain bound to atoms, and the band gap is the energy difference between these two bands. The photons with energy greater than the band gap can be absorbed by the semiconductor, resulting in the excitation of electrons from valence band to the conduction band. Thus, the light absorption occurs at specific wavelength corresponding to the bandgap of the

semiconductor. The band gap (E_g) is exactly equal to the energy difference of the lowest conduction band edge and the highest valence band edge. Regarding to the excitation of electrons from VB to CB, there are two types of interband transitions: direct and indirect transitions. For direct transition, the phonon is not required since the momentum is conserved. For the indirect transition, the phonon is required to conserve the momentum in the absorption or emission process. These two types of transition can occur in all semiconductors. The detailed illustration of the electron transition is shown in Figure 2.2, here the direct forbidden transition barely occurs in the semiconductor [92].

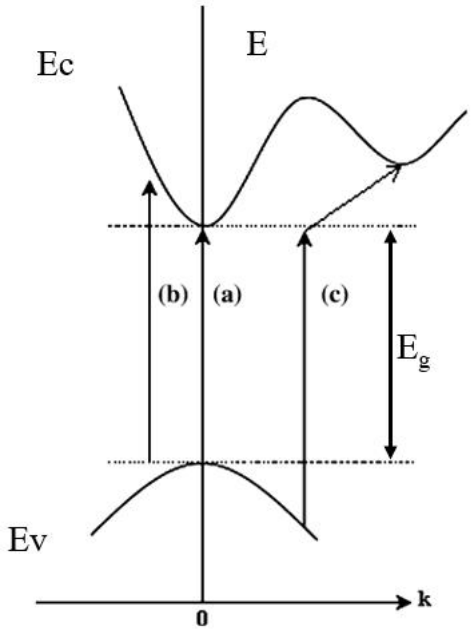

Figure 2.2 Band transition illustration: (a) allowed and (b) forbidden direct gap absorption of a photon with E_g energy (c) for the indirect gap, the assistance of a phonon is required [92]

The band gap is a significant parameter to evaluate the optical properties of semiconductor, and there is difference between the bandgap of bulk material and nanostructure. The band gap can be affected by many factors, such as synthesis conditions [93,94], mismatch between the substrate and semiconductor [94,95] ,

annealing temperature [96,97], composition [96,98,99], crystallite size and film thickness [100]. There are many techniques can be used to evaluate the band gap of the nanomaterial namely photoluminescence spectroscopy (PL) [101], ultraviolet–visible near-infrared spectroscopy (UV–vis–NIR) [102], valence electron energy-loss spectroscopy (VEELS) [103], incident photon conversion efficiency (IPCE) spectra [104] and theoretical calculation using density functional theory (DFT) [105]. The first two are the common techniques that have been widely used for researchers, among which the UV–vis–NIR is the most preferred and cheapest method for the band gap determination.

The UV–vis–NIR spectroscopy technique cannot be influenced by the electrical conductivity, photoconductivity of the samples and also is independent on the temperature. This technique can give information about the transitions of electrons between different orbitals of the material by identifying the type of orbitals. For absorption spectroscopy, the curve will display an exponential drop at specific wavelength which suggest the most appropriated method to calculate the bandgap of the semiconductor. In 1958, Shapiro first reported the measurement of band gap through the extrapolating the linear portion of the absorption curve with the wavelength axis [106]. In the curve, the linear segment corresponds to the fundamental interband transition, while the nonlinear segment presents the electron transition of the band tail [107]. The diffuse reflectance spectroscopy used for the determination of bandgap through the linear section in the solid is highly justified. Primarily, Kubelka and Munk tried to study the colour change of the substrate with a paint layer with a theoretical assumption in 1931 [108]. At present, the Kubelka-Munk model (K-M) has been widely employed to analyse the result of diffuse reflectance spectroscopy for the determination of the band gap of semiconductor.

In the UV–vis–NIR system, the sample is illuminated with the diffuse monochromatic radiation that the absorption and scattering occur at the same time. The area of the sample in research is A and the thickness is L. The intensity of the incident light is I, the reflectance light has the intensity of J, then the reflectance can be defined as R= J/I which is a dimensionless quantity. Moreover, the reflectance R depends on the thickness, absorption and scattering properties of the sample. The widely recognized formula for the (K-M) model is shown as follows:

$$F(R) = \frac{(1-R)^2}{2R} = \frac{\alpha}{S}\# \qquad 2.1$$

Where α is the absorption coefficient, R is reflectance, S is the scattering coefficient. Since the quantity R is dimensionless the function F(R) also is dimensionless. This equation is based on the assumption that the sample has a semi-infinite thickness and the reflectance of the sample is always the same amount regardless of the type of the substrate. Murphy emphasized that the thickness of 1-3mm is needed for the sample [104]. Meanwhile, the Escobedo-Morales *et al.* ever pointed that to avoid the impact from the substrate, thickness over 2mm is required for the sample ready for the measurement [93]. The absorption and scattering coefficient are the intrinsic properties of the material, which indicate the possibility of light absorption and scattering per unit path length. The absorption is essentially for every material while the scattering is affected by the inhomogeneity. Besides, the scattering is independent on the light absorption. This model is not only suitable for one direction light propagation, but also for three-dimensional light diffuse phenomenon when L is infinite, the scattering is isotropic and the medium is homogeneous [109].